ACS APPLIED MATERIALS & INTERFACES

Research Article

www.acsami.org

Mechanism of Graphene Oxide as an Enzyme Inhibitor from Molecular Dynamics Simulations

Xiaotian Sun,[†] Zhiwei Feng,[†] Tingjun Hou, and Youyong Li*

Institute of Functional Nano & Soft Materials (FUNSOM) and Collaborative Innovation Center of Suzhou Nano Science and Technology, Soochow University, Suzhou 215123, China

Supporting Information

ABSTRACT: Graphene and its water-soluble derivative, graphene oxide (GO), have attracted huge attention because of their interesting physical and chemical properties, and they have shown wide applications in various fields including biotechnology and biomedicine. Recently, GO has been shown to be the most efficient inhibitor for α-chymotrypsin (ChT) compared with all other artificial inhibitors. However, how GO interacts with bioactive proteins and its potential in enzyme engineering have been rarely explored. In this study, we investigate the interactions between ChT and graphene/GO by using molecular dynamics (MD) simulation. We find that ChT is adsorbed onto the surface of GO or graphene during 100 ns MD simulations. The α-helix of ChT plays as an important anchor to interact with GO. The cationic and hydrophobic residues of ChT form strong interactions with GO, which leads to the deformation of the active site of ChT and the inhibition of ChT. In comparison, the active site of ChT is only slightly affected after ChT adsorbed onto the graphene surface. In addition, the secondary structure of ChT is not affected after it is adsorbed onto GO or graphene surface. Our results illustrate the mechanism of the interaction between GO/graphene and enzyme and provide guidelines for designing efficient artificial inhibitors.

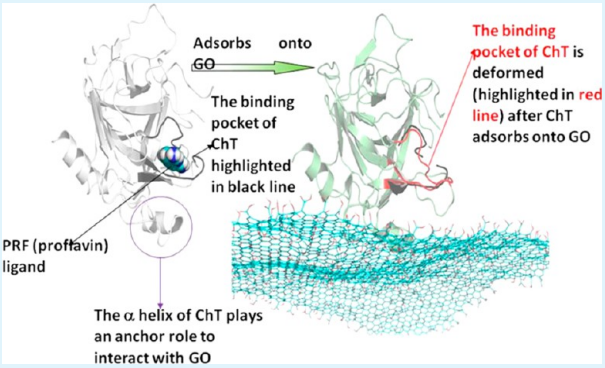

KEYWORDS: *graphene oxide, enzyme, inhibitor, molecular dynamics*

INTRODUCTION

Enzymes are large biological molecules that regulate almost all chemical reactions in numerous biological processes, including signal transduction, gene expression, immune responses, metastasis, and metabolism. Moreover, enzymes are widely used in the pharmaceutical and medical fields, food and environmental industry, biofuel area, as well as life science studies.[1,2] Therefore, regulation of enzyme activity and stability is very important and has always attracted great attention. Various enzyme regulators, ranging from proteins, peptides, and synthetic organic molecules, have been discovered in the recent years.

Recently, accompanying the development of nanostructured materials, a range of nanomaterials with different sizes and shapes have been utilized as the substrates for enzyme modulation. Different types of nanomaterialshave been reported to show positive effects on enzymes, including gold nanoparticles,[3−8] magnetite nanoparticles,[9] alumina nanoparticles[10,11] and porous silica structures,[12−14] yet mostly through enzyme immobilization process.[15]

Enzymes immobilized on the nanostructured materials have some advantages[16,17] over the bulk solid substrates, including enhance the stability, repeat or continuous use, easy separation from the reaction mixture, possible modulation of the catalytic properties, prevention of protein contamination in the product, easier prevention of microbial contaminations, etc. However, to efficiently immobilize enzymes on nanostructured material surfaces, labored work is required to modify/functionalize the substrate surface.[18,19] Last but not least, it is hard for most nanostructured materials to fully characterize their surfaces by using conventional surface analytical tools.

Graphene oxide[20−23] (GO) is an ideal substrate for enzyme immobilization on nanostructured materials: GO is enriched with oxygen-containing groups, which makes it possible to immobilize enzymes without any surface modification or coupling reagents.

In the past few years, graphene and its water-soluble derivative-GO have attracted huge attention because of their interesting physical and chemical properties, which also show wide applications in various fields including biotechnology and biomedicine. GO, in particular, possesses a single-layered, two-dimensional, sp^2 hybrid structure with sufficient surface groups, offering a unique double-sided, easily accessible substrate for multivalent functionalization and efficient loading of molecules from small organic ones to biomacromolecules. Functionalized GO is potential for applications in gene and drug delivery,[24]

Received: January 9, 2014
Accepted: May 6, 2014
Published: May 6, 2014

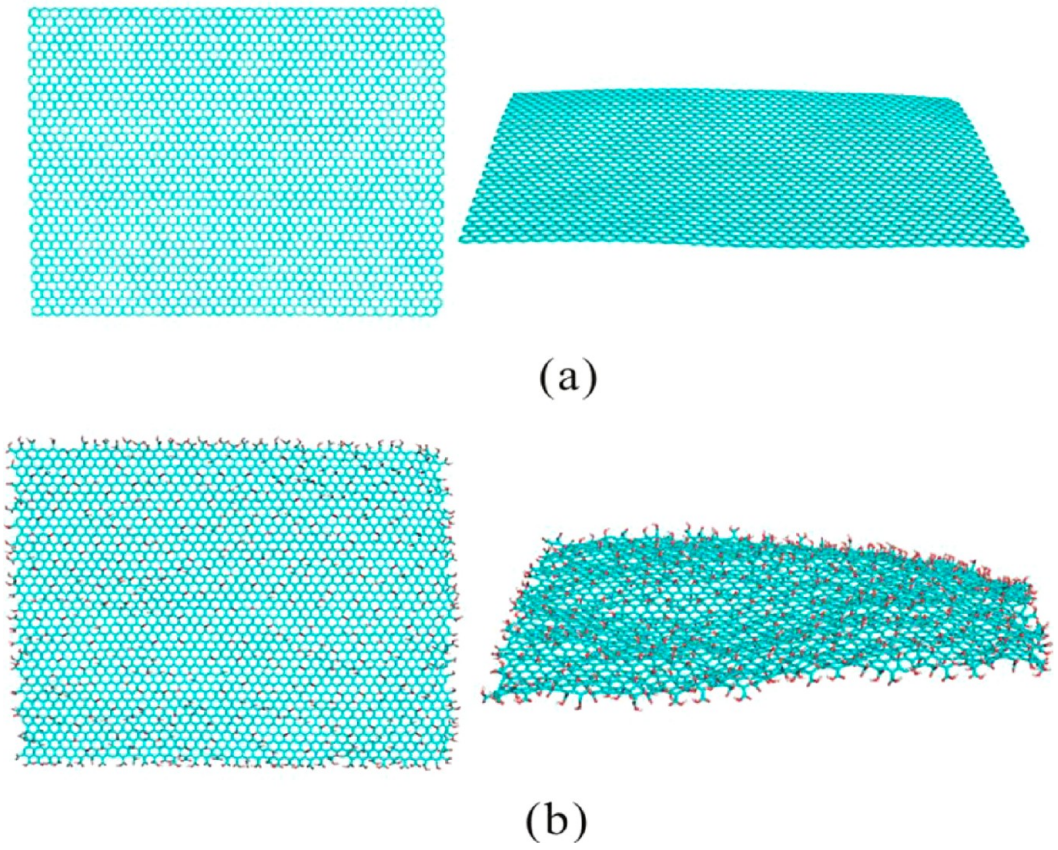

Figure 1. Atomic structures of (a) graphene (size 10.0 × 9.0 nm^2) with 3115 carbon atoms and (b) GO modified from graphene.

cellular imaging,[25] cancer therapeutics,[26] biosensing,[27] as well as antibacterial agent.[28] For instance, the GO nanosheets modified with poly(ethylene glycol) have been employed as aqueous compatible carriers for water-insoluble drug delivery.[4] The intrinsic oxygen-containing functional groups were used as initial sites for deposition of metal nanoparticles and organic macromolecules, such as porphyrin, on the GO sheets, with opened up a novel route to multifunctional nanometer-scaled catalytic magnetic and optoelectronic materials.

Regarding the interactions between GO and biomacromolecules, such as enzymes, GO has been reported in a few studies.[29,30] In a recent work, De et al.[31] uncovered that GO could act as an artificial modular to inhibit the activity of α-chymotrypsin (ChT) and it showed the highest inhibition dose response (by weight) for ChT inhibition compared with all other reported artificial inhibitors. However, the mechanism of GO bound with ChT at atomic level is still unclear.

Therefore, in this study, we employ MD simulations to investigate the dynamic interactions between graphene/GO and ChT. Our results show that ChT is adsorbed onto the surfaces of both graphene and GO. The cationic and hydrophobic residues of ChT form strong interactions with GO, leading to the deformation of the active site of ChT and the inhibition of ChT. However, the active site of ChT is only slightly affected after it adsorbed onto the graphene surface. These findings suggest a new generation of enzymatic inhibitors that can be applied to other complex proteins by systematic modification of the GO functionality.

MATERIALS AND METHODS

Atomic Structures. The crystal structures of ChT[32] (PDB entry: 4CHA, resolution 1.68 Å) and trypsin[33] (PDB entry: 1TRN, resolution 2.20 Å) used in our studies are retrieved from the Protein Data Bank (http://www.pdb.org/pdb/). The crystal structures are then prepared by Discovery Studio 2.5 (DS2.5). Missing atoms are added and the protein is minimized in DS2.5. DS2.5[34] is used to determine the protonated states for histidines and other residues within the physiological pH range (~7.4): Electrostatic interaction energies are calculated using an implementation of Generalized Born solvation model in CHARMM and the atomic parameters are taken from either CHARMM or CHARMM polar hydrogen force fields. The energies of the protonated and deprotonated states are calculated and the percentage of protonation of each residue is predicted at given pH on the basis of the Boltzmann distribution.

For ChT, the calculated pK_a values of the histidines are 9.073 for His40, and 9.395 for His57. We then use PROPKA 3.1[35] and H++ 3.0[36] to predict pK_a of His57:7.31/8.70 for His57. Thus, His40 and His57 of ChT are protonated.

For trypsin, the calculated pK_a values of the histidines are 7.863 for His40, 9.439 for His57, and 5.791 for His91. We also use PROPKA 3.1[35] and H++ 3.0[36] to predict the pK_a value of His57:7.10/7.55 for His57. Thus, His40 and His57 of trypsin are protonated.

Side chains of Asp, Glu, Arg, and Lys were charged (Asp^-, Glu^-, Arg^+, and Lys^+) in all simulations.

In the literature,[37−40] pK_a values of His57 determined by various experimental studies and computational studies range between 6 and 7. Our calculation results above show that pK_a value of His57 ranges between 7.0−9.5. Thus, we first perform MD studies with protonated His57. We also perform MD studies with neutral His57. Both MD studies show that His57 is far away from the interface between ChT and GO/graphene. And the protonation state of His57 does not affect the interaction between ChT and GO/graphene significantly. See the

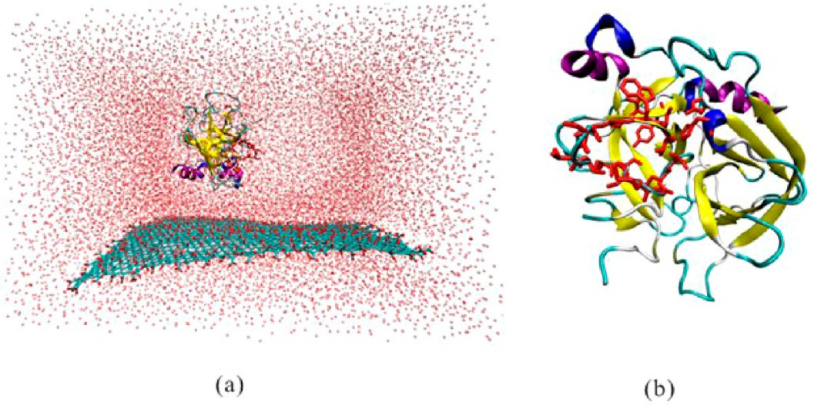

Figure 2. (a) MD simulation box of GO and ChT with water (the orientation of ChT is randomly selected); (b) active pocket of ChT highlighted in red.

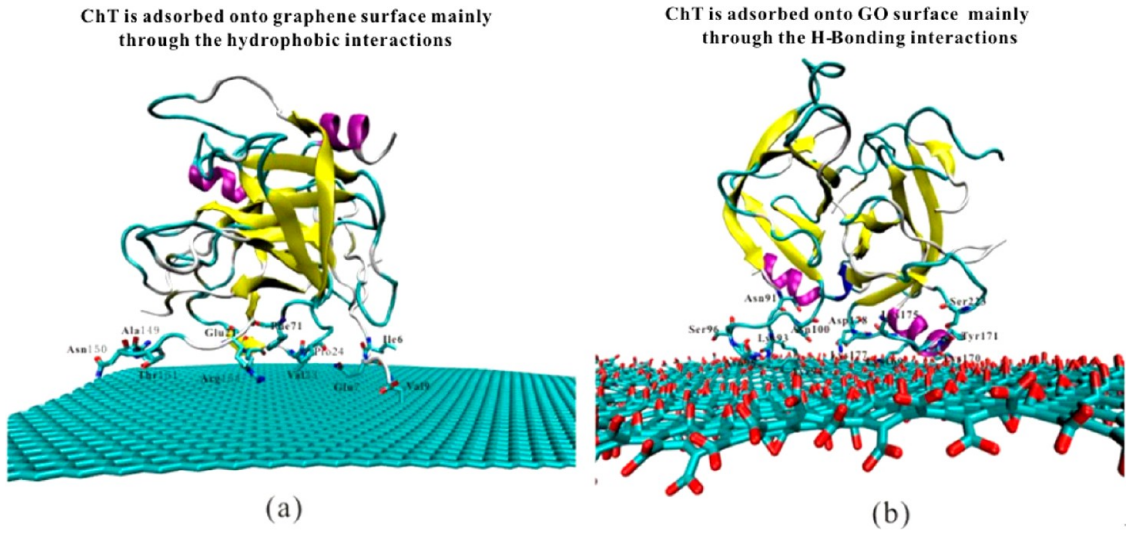

Figure 3. Typical structure of α-chymotrypsin adsorbed onto (a) the graphene surface and (b) the GO surface. Three randomly selected orientations of ChT lead to three different interaction modes of ChT with graphene/GO, the other two can be found in Figure S1 in the Supporting Information.

section "MD results of ChT with neutral His57 show similar results as ChT with protonated His57".

We prepare the graphene sheet with size of 10.0 × 9.0 nm^2 (3,115 carbon atoms, Figure 1a), which provides a sufficient large surface for the enzyme to be adsorbed onto it. The epoxy and hydroxyl groups are randomly grafted to the carbon atoms on the graphene basal plane. The carboxyl groups are also attached to the carbon atoms on the edge randomly. The GO model considered here is not significantly oxidized: $C_{10}O_1(OH)_1$ (i.e., 1 epoxy group and 1 hydroxyl group per 10 carbon atoms are attached to the graphene basal plane), as shown in Figure 1. This GO model reflects a typical outcome from a standard oxidation process.[23,41−43] One carboxyl group per 20 carbon atoms is attached to the graphene edge ($C_{10}O_1(OH)_1(COOH)_{0.5}$) to mimic the behavior of GO in neutral or high pH condition.

Then, the GO structure is prepared by Material Studio 5.5. Geometry optimization is performed by using the Forcite module with the Dreiding force field[44,45] and the Gasteiger charges[46] (the maximum iteration is set to 50 000 and the convergence is set to 5.0 × 10^{-6}) and the ultrafine quality is used for the energy calculation. The minimized structure (Figure 1b) is regarded as the initial structure of GO for the following simulations.

MD Simulations. The carbon atoms of graphene/GO are uncharged according to Hummer et al.[47] Graphene/GO is fixed during the simulations. The initial minimum distance between the graphene/GO surface and protein is 2.0 nm. The enzyme and graphene/GO do not contact in the beginning of the simulations. We randomly select three orientations of the enzyme and perform three independent MD simulations. In the randomly selected orientations, the active pocket of ChT is facing away from the graphene/GO surface as shown in Figure 2.

Then, the protein and graphene/GO are embedded into a rectangular box of TIP3P water molecules[48] with a size of 11.0 × 10.0 × 7.5 nm^3, and the waters within 5/2 Å of the protein/graphene are eliminated. Five angstroms is a reasonable criterion, because the favorable Van Der Waals interaction distance is between 4 and 5 Å. The simulation systems are built up by using VMD.[49]

The whole system (Figure 2) contains the protein (ChT/trypsin), graphene/GO, ~29 688/27 071 water molecules, and 123/121 sodium ions for a total of ~97 009/88 874 atoms per periodic cell. The system is first equilibrated for 200 ps with the protein fixed. Then, the protein is released and another 200 ps equilibration is performed, which there is no vacuum left in the systems.

Starting from the last frame of the equilibration, we perform 100 (or 50 for ChT with deprotonated His57) ns NPT MD simulations using the NAMD package[50] (version 2.7b2) with CHARMM27[51−53] force field. In addition, Dreiding force field is used to describe the interactions between the graphene/GO and protein. Dreiding force field is useful for predicting structures and dynamics of organic, biological and main-group inorganic molecules, which leads to accurate geometries and reasonably accurate barriers for various organic systems and widely used for the MD simulations. Long-range electrostatics is handled by the particle mesh Ewald (PME) method[54]

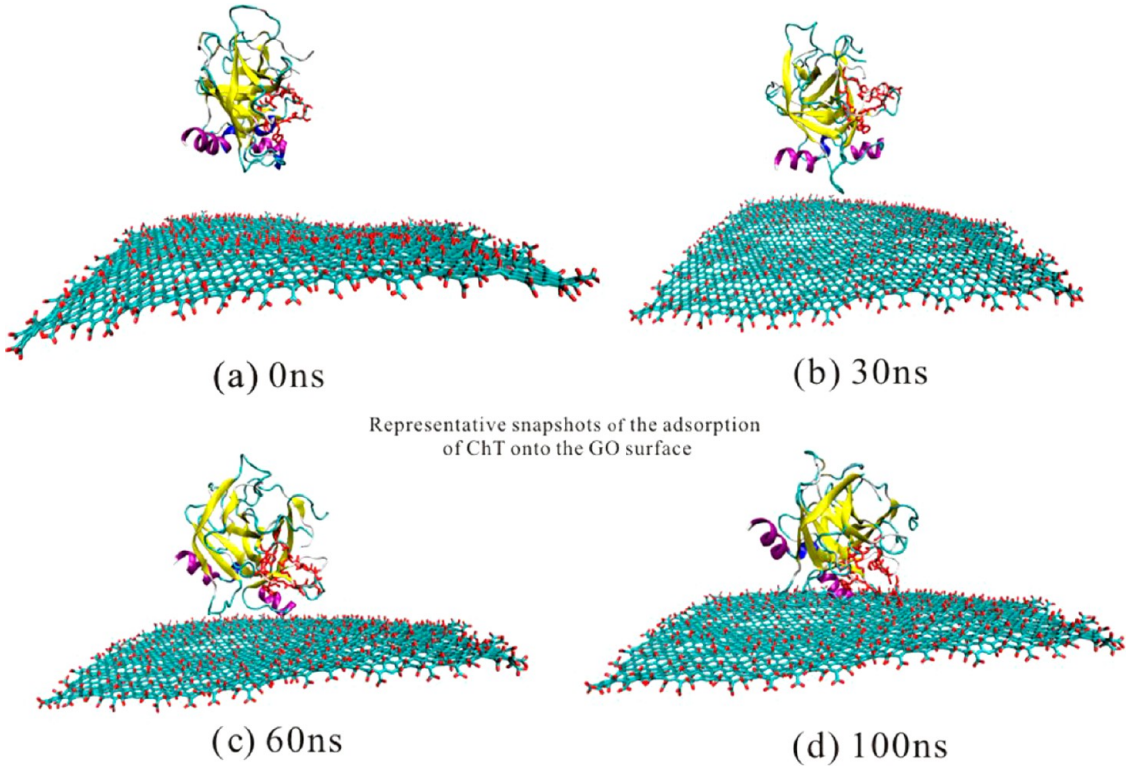

Figure 4. Representative snapshots of the adsorption of ChT onto the GO surface (a) 0, (b) 30, (c) 60, and (d) 100 ns extracted from the MD trajectory. The S1 active site of ChT is highlighted in red.

with a 12 Å nonbonded cutoff and a grid spacing of 1 Å per grid point in each dimension. The Van Der Waals energies are calculated using a smooth cutoff (a switching radius of 10 Å and a cutoff radius of 12 Å). The constant temperature of 310 K and the constant pressure of 1 atm are applied by a langevin thermostat and a langevin barostat, respectively. The time step of the MD simulations is set to 1 fs, and the snapshots are saved every 10 ps. The trajectory analyses are carried out with VMD.

Dock Proflavine (PRF) into ChT. To examine the change of the active site of ChT after ChT is adsorbed onto graphene/GO, we predicted the 3D model of proflavine in complex with ChT by using the CDocker program in DS2.5. The docking site is set at the center of the active pocket of ChT with a radius of 10 Å, large enough to cover the whole binding pocket. CDocker is a grid-based molecular docking method that employs CHARMM force field. The receptor is rigid, whereas the ligands are flexible during the refinement. Random ligand conformations are generated from the initial ligand structure through high temperature molecular dynamics, followed by random rotations. The random conformations are refined by grid-based simulated annealing and a final grid-based or full force field minimization.

The following parameters are used for the dockings: CHARMM force field is used, Grid extension is set to 8.0, 50 random conformations of each ligand are generated, simulated annealing refinement is performed: 2000 steps for heating and 5000 steps for cooling, and 100 binding poses are saved for each ligand.

RESULTS AND DISCUSSIONS

Adsorption of α-Chymotrypsin onto Graphene or GO. The dynamic features of the ChT-GO/graphene interactions in explicit water are explored by the MD simulations. After 100 ns MD simulations, we find that ChT is adsorbed onto the surface of graphene or GO. As shown in Figure 3a and Figure S1a in the Supporting Information, three randomly selected orientations of ChT lead to three different interaction modes with graphene. However, three randomly selected orientations of ChT lead to consistent interaction patterns with GO as shown in Figure 3b and Figure S1b in the Supporting Information. The initial minimum distance between graphene/GO surface and ChT is 2.0 nm (Figure 2). Along the MD simulations, ChT is gradually adsorbed onto the surface of graphene or GO. At 100 ns, the average minimum distance between graphene and ChT is ~1.86 Å, whereas the average minimum distance between GO and ChT is ~0.85 Å. Similar observations are observed by the recent simulation reports: peptides (GAM peptide, dodecamer peptide, α-helical peptide, and RC7 peptide) and proteins (fibronection module, insulin, HP35, WW domains, and human serum albumin) can be adsorbed onto the surface of graphene,[55,56] carbon nanotube,[55,57−59] C60,[55,60] and gold nanoparticles.[3,4,6]

As shown in Figure 3a and Figure S1a in the Supporting Information, ChT shows different interaction modes with graphene in three independent MD runs, but hydrophobic residues always contribute most to the interaction with graphene: the adsorption area of ChT onto graphene is only ~8.6 nm^2, because of the "flat surface" of graphene. A variety of hydrophobic residues contribute to the adsorption of ChT onto graphene, which include Ile6, Val9, Val23, Pro24, and Ala149. Moreover, the aromatic residue Phe71 contributes $\pi-\pi$ stacking and CH$-\pi$ interactions with graphene surface. The distances between these residues and the graphene surface are less than 1.5 Å.

However, it is completely different for the adsorption of ChT onto the GO surface (Figure 3b and Figure S1b in the Supporting Information). Three randomly selected orientations of ChT lead to consistent binding patterns with GO. In all three simulations the α-helix consisted of the residues 165 to 172 is adsorbed onto the surface of GO. Importantly, almost all residues interacting with GO are hydrophilic residues, especially

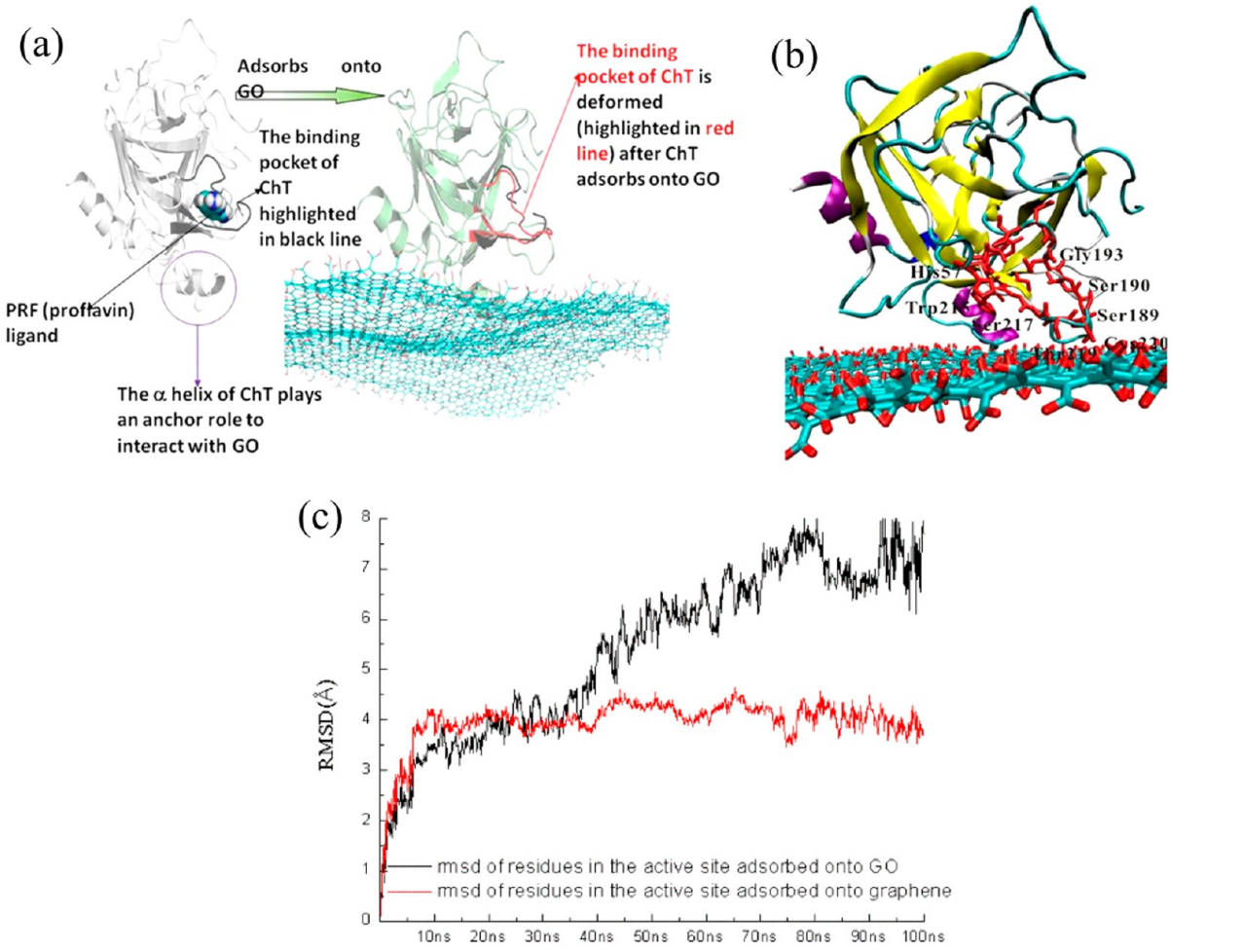

Figure 5. (a) Active site of ChT is deformed after ChT is adsorbed onto the surface of GO, which the α-helix of ChT plays as an important anchor to interact with GO; (b) active site of S1 from one of the MD simulation; (c) average rmsd of the active site of ChT during the 100 ns MD simulations with GO (black line) or graphene (red line).

lysine and asparagine. These residues in ChT prefer the oxidized part of GO. Therefore, ChT is prone to be adsorbed onto the oxidized part of GO.

Our results show that ChT is favored with the "concave surface" of GO, which has large surface curvature and area. So, the adsorption area of ChT onto GO is ~12.3 nm^2. Importantly, the residues directly interacting with GO surface are all hydrophilic residues, which include Asn91, Lys93, Tyr94, Asn95, Ser96, Asn100, Lys169, Lys170, Tyr171, Lys175, Lys177, Asp178, and Ser223. These hydrophilic residues form strong hydrogen bonds with epoxide and/or carbonyl groups on the surface of GO. Particularly, lysines from ChT are cationic residues, which form favorable interactions with anionic graphene oxide.

S1 Specificity Pocket in ChT is Deformed after It Is Adsorbed onto the GO Surface. ChT is composed of 245 residues (M_w of 25 kDa), which contains in three separate polypeptide chains linked by five disulfide bridges. The catalytic site of ChT can be divided into four distinct regions: the n-site where the nucleophilic attack occurs; the $\alpha\gamma$-site, a deeply invaginated apolar pocket close to the active serine, which binds aromatic side chains; the am-site (amide), which can form H-bonding interactions with substrate; and the h-site, which accommodates the α-hydrogen of substrates. The $\alpha\gamma$-site, known as the S1 specificity pocket (residues 189–195, 213–220 and 226–228), is the most important binding locus that controls directly the specificity and efficiency of the enzyme, as shown in Figure S2 in the Supporting Information. The catalytic triad, formed by His57, Asp102, and Ser195, has been described as a charge relay system in which the relative proximity of Asp102 to His57 serves to polarize the hydrogen bonding network between the imidazole ring of His57 and the hydroxyl proton of Ser195. The active serine from the catalytic triad (Ser195) is located at the mouth of the S1 cavity. The deeply invaginated hydrophobic S1 pocket of ChT shows high specificity for aromatic (Phe, Trp, Tyr) and bulky apolar side-chains.[61]

Our results show that when ChT interacts with graphene, the active site of S1 in ChT is far away from the graphene surface in all three independent MD simulations (see Figure S3a in the Supporting Information). The average center-of-mass distance between the active site of S1 in ChT and the graphene surface is 18.6 Å. Moreover, the minimum distance between the residues in the active site and graphene is ~7.2 Å. By using sitemap module in Schrodinger, we estimate that the volume of the active site of ChT changes from 146.1 $Å^3$ (crystal structure) to 130.0 $Å^3$ (average value from three independent MD runs) after the adsorption of ChT onto graphene surface. These results support the fact that the interaction with graphene will not affect the S1 binding pocket of ChT significantly.

dx.doi.org/10.1021/am500167c | ACS Appl. Mater. Interfaces 2014, 6, 7153–7163

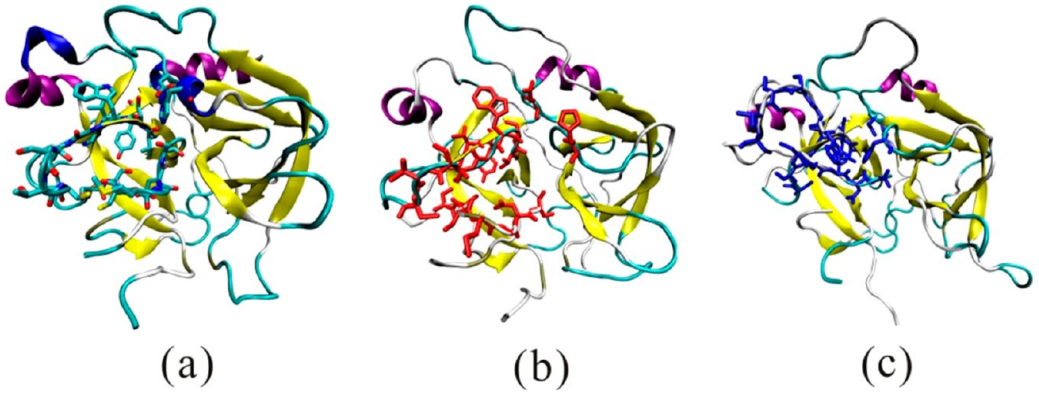

Figure 6. Comparison of the conformations in (a) the crystal structure of ChT, (b) in the structure absorbed onto the graphene surface, and (c) in the structure adsorbed onto the GO surface.

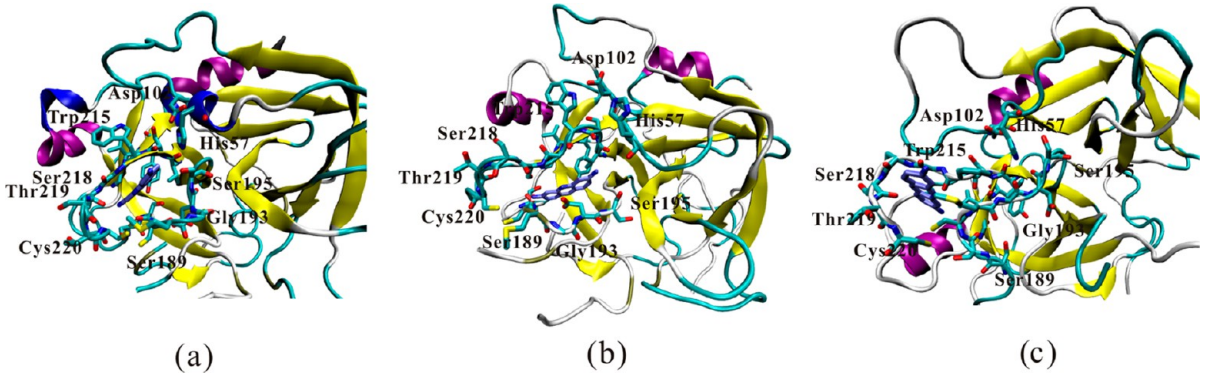

Figure 7. Conformations of the active site of ChT (a) in the crystal structure, (b) in the structure adsorbed onto graphene, and (c) in the structure adsorbed onto GO. Figures on the left show the conformations of the ChT-proflavine complexes, and figures on the right show the binding sites of ChT.

However, our results show that the active site of S1 in ChT adsorbed onto GO. Figure 4 shows representative snapshots of the adsorption for S1 onto the GO surface. First, the enzyme gets close to the surface of GO (~30th ns) due to cationic residues of ChT (long-range Coulomb interactions between ChT and GO). Then, the α-helix consisting of the residues 165−172 is adsorbed onto the surface of GO (~60th ns), which behaves as an "anchor". Finally, the active site is adsorbed onto the GO surface.

Moreover, our results show that the active site of S1 in ChT will be affected significantly when ChT interacts with GO, as shown in Figure S3b in the Supporting Information. By using sitemap module in Schrodinger, we estimate that the volume of the active site of ChT changes from 146.1 Å^3 (crystal structure) to 75.8 Å^3 (average value from three independent MD runs) after the adsorption of ChT onto GO surface.

Importantly, our results show that the α-helix (consisted of the residues 165 to 172, sequence: "TNCKKYW") is strongly adsorbed onto the GO surface in all three independent MD simulations. Five of seven residues are hydrophilic, and one residue (Trp172) is aromatic. Trp172 close to the binding site is proposed to be responsible for the induced circular dichoroism (CD) activity.[62] Five hydrophilic residues can enhance the interaction between ChT and GO, whereas the aromatic residue (Trp172) contributes the $\pi-\pi$ stacking and CH$-\pi$ interactions.

Figure 5a indicates that in three independent simulations, the S1 active site of ChT is deformed after ChT is adsorbed onto GO, which blocks the S1 active site and inhibits ChT.

From Figure 5b, we can clearly observe that the active site of S1 from one MD simulation is significantly affected by the interaction with GO. Most residues of the active site interact strongly with GO. The catalytic triad (His57, Asp102 and Ser195) is directly adsorbed onto GO. Moreover, Trp215, another aromatic residue, forms a strong $\pi-\pi$ interaction with GO. This residue near to the binding site is also proposed to be responsible for the induced circular dichoroism (CD) activity.[62] Importantly, several hydrophobic residues of the active site (including Met192, Val213, Cys220, and Val227) contribute hydrophobic interactions. Finally, a ring of positively charged residues around its active pocket interacting with anionic ions of GO (Lys93, Lys169, Lys170, Lys175, and Lys177). The strong interaction between ChT and GO deforms the active site of ChT, leading to the inhibition of ChT.

Figure 5c shows the average rmsd of the active site of ChT during the 100 ns MD simulations with GO (black line) or graphene (red line). We can see that the active site of ChT is affected significantly by the absorption with GO, but is not by the absorption with graphene.

To further elucidate how the deformed active site inhibits the enzymatic activity, we used the CDocker program to dock proflavine into three structures (the crystal structure of ChT, the structure adsorbed onto graphene with lowest deviation during three independent MD simulations, and the structure absorbed onto GO with lowest deviation during three independent MD simulations). The results are discussed in the following section.

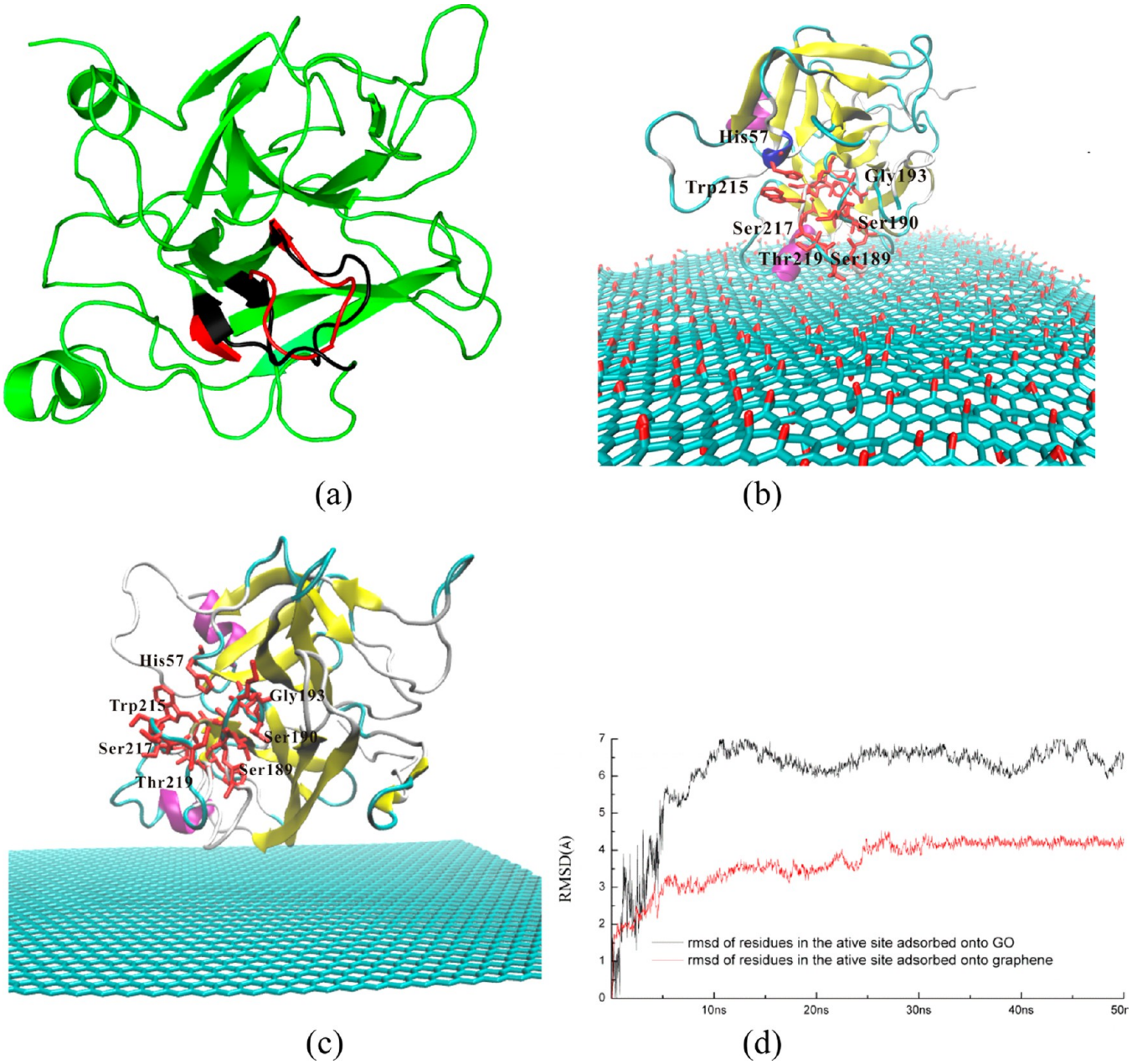

Figure 8. (a) Active site of ChT with deprotonated His57 is deformed after ChT is adsorbed onto the surface of GO (highlighted in red), (b) active site of S1 is adsorbed onto GO, (c) active site of S1 is far away from the surface of graphene, (d) rmsd of the active site of ChT during the 50 ns MD simulations with GO (black line) or graphene (red line).

Active Site of ChT Is Deformed after Adsorbing onto GO. Conformation of active site is the most important binding locus which controls the specificity and efficiency of an enzyme. In this section, we want to examine how the conformational changes of the active site for ChT when ChT interacts with graphene or GO.

From Figure 6a–c, different degrees of conformational changes can be found for the active site. For the structure of ChT absorbed onto graphene (Figure 6b), the region consisted of His57, Asp102, Gly193, Asp194, Ser195, Trp215, and Glu216 (here we named it the proximal region), becomes larger, whereas the rest region (we named it the remote region) becomes narrower. However, the binding pocket of the active site is large enough for ligand binding.

However, for the structure of ChT adsorbed onto GO (Figure 6c), the proximal region is almost covered, while the remote region can allow only some small ligands to be docked vertically into it.

To accurately characterize the conformational change of the active site before and after the prolonged graphene/GO binding, we predict the binding mode of proflavine in complex with ChT[63] by using the CDocker program in DS2.5. We first dock proflavine into the crystal structure of ChT, as shown in Figure 7a. This binding mode of ChT-proflavine ranks first among the 100 top hits, and it is also in agreement with the recent docking reports.[61,63] The docking score between the crystal structure and proflavine is −21.82 kcal/mol (CDOCKER_INTERACTON_ENERGY). Our results show that the binding site is large enough for accommodating the ligand.

dx.doi.org/10.1021/am500167c | ACS Appl. Mater. Interfaces 2014, 6, 7153–7163

Moreover, proflavine is favored with the proximal region of the active site, and it directly interacts with His57, Asp102, and Ser195 in a catalytic triad.

We then dock proflavine into the structure of ChT adsorbed onto graphene, as shown in Figure 7b. The docking scores of CDOCKER_INTERACTON_ENERGY between the ChT adsorbed onto graphene and proflavine are −23.77, −19.56, and −17.74 kcal/mol, respectively. These docking scores are close to that of crystal structure of ChT and proflavine. Our results illustrate that two of three binding sites are similar to that of the crystal structure, while the binding site of the last one is mainly located in the proximal region. However, all three binding sites are large enough to allow ligands to be bound into, especially the proximal region of the active site, the region of catalytic triad. From Figure 7b, we can find that the residues His57, Asp102, Ser195, and Trp215 move opposite to the center of the active site, which makes the proximal region larger. Meanwhile, Ser189 gets closer to Ser217 in the remote region, making the remote region of the active site narrower. However, the conformation of the whole active site is similar to that of the crystal structure.

We also dock proflavine into the structure of ChT adsorbed onto GO (Figure 7c). We only have two binding modes in this system (Figure 7c shows one of them), because one of the three active sites is completely covered. The docking scores of CDOCKER_INTERACTON_ENERGY between ChT adsorbed onto GO and proflavine are 48.53 and 60.46 kcal/mol. These two docking scores show very weak binding between ChT adsorbed onto GO and proflavine. These two binding modes share large similarities in the proximal region of the active site (Figure 7c): three residue pairs including His57-Ser195, Asp102-Asp194 and Trp215-Gly193, move closer to each other and cover the proximal region of the active site, making most of the active site not be available for the ligand; moreover, the motif consisted of the residues 189 to 191, moves away from the original position strongly; meanwhile, the motif consisted of the residues 217 to 220 also has large conformational change, approaching to the previous motif. Although the remote region becomes larger, it can only allow the small ligand be docked into vertically. However, the conformational changes of both the proximal region and the remote region make the active site not suitable for most ligands.

In summary, for the structure of ChT absorbed onto the graphene surface, the active site is far away from the surface of graphene, and the whole active site of S1 of ChT is similar to that of the crystal structure (especially the proximal region of the catalytic triad). However, in the structure of ChT absorbed onto GO, the whole region of the active site is unavailable for ligands with large conformational change, which strongly inhibits the activity of ChT. Moreover, our simulations also show that the active site of ChT is faced and adsorbed onto the GO. We suggest that another potential inhibiting effect of ChT is the active site of ChT is not available, which it is blocked by GO.

MD Results of ChT with Neutral His57 Show Similar Results as ChT with Protonated His57. In many experimental and computational studies,[37−40] the pK_a value of His57 is between 6 and 7. Thus, we also perform 50 ns MD studies with neutral His57. The results are shown in Figure 8. MD studies with neutral His57 or protonated His57 show that His57 is far away from the interface between ChT and GO/graphene. And the protonation state of His57 does not affect the interaction between ChT and GO/graphene significantly.

Our results also show that ChT with deprotonated His57 is also adsorbed onto graphene and GO. Figure 8a indicates that in ChT with deprotonated His57, the S1 active site is deformed after ChT is adsorbed onto GO, comparing with the ChT adsorbed onto graphene. The volume of the active site of ChT (with deprotonated His57) adsorbed onto graphene changes from 146.1 Å^3 (crystal structure) to 134.7 Å^3. In comparison, the volume of the active site of ChT (with deprotonated His57) adsorbed onto GO changes from 146.1 Å^3 (crystal structure) to 109.4 Å^3.

Figure 8b shows that the active site of S1 is significantly affected by the interaction with GO. Most residues of the active site also interact strongly with GO, including Ser189, Ser217, Thr219, and Cys220. In comparison, His57 is far away from GO. These results agree with our previous MD results with protonated His57.

Figure 8c shows that the active site of S1 in ChT with deprotonated His57 is far away from the surface of graphene.

Figure 8d shows the rmsd of the active site of ChT with deprotonated His57 during the 50 ns MD simulations with GO (black line) or graphene (red line). The figure shows that the active site of ChT with deprotonated His57 is also affected significantly by the absorption with GO, but is not affected by the absorption with graphene.

In conclusion, our MD results of ChT with neutral His57 show similar results as ChT with protonated His57.

In order to validate further these results, we also perform the MD simulations for trypsin in the following section.

Similar Results on the Adsorption of Trypsin. Trypsin, another serine protease, has an evolutionary history with ChT (including the S1 active site), and it shares the sequence identity of 41% and sequence similarity of 60% with ChT. We perform 100 ns MD simulation of both adsorption onto graphene and GO, and also dock the active ligand into three structures of trypsin (the crystal structure of trypsin, the structure absorbed onto graphene, and the structure absorbed onto GO). The initial minimum distance between graphene/GO and trypsin is also 2.0 nm. The binding site (or binding mode in the active site) of the crystal structure of trypsin is very similar to that of ChT.

Our results show that trypsin is adsorbed onto the surface of both graphene and GO (Figure 9). Moreover, our results illustrate that the S1 pocket in trypsin is far away from graphene, which is absorbed by hydrophobic interactions. However, the active site is adsorbed onto the GO surface through its cationic residues and hydrophilic residues (Figure 9). Importantly, the ligand can be docked into the active site of trypsin adsorbed onto graphene (Figure 9b). On the other hand, the active site of trypsin adsorbed onto GO is covered and the catalytic triad cannot interact with ligand any more (Figure 9c). All these results are in good agreement with our results for ChT.

However, differences can be found between trypsin and ChT. Both for the trypsin adsorbed onto graphene and GO, we can find that the motif composed of the residues 215−220 divides the active site into two parts: one part consists of the residues 215−228 (we named it the left region), and the other part consists of the residues 189−195, His57, Asp102, and residues 215−220 (we named it the right region), as shown in the middle of Figure 9c. Moreover, the ligand bound with the structure absorbed onto graphene can interact with the catalytic triad, but the main part of the ligand can be found in the left region (in the middle of Figure 9b). However, the ligand bound

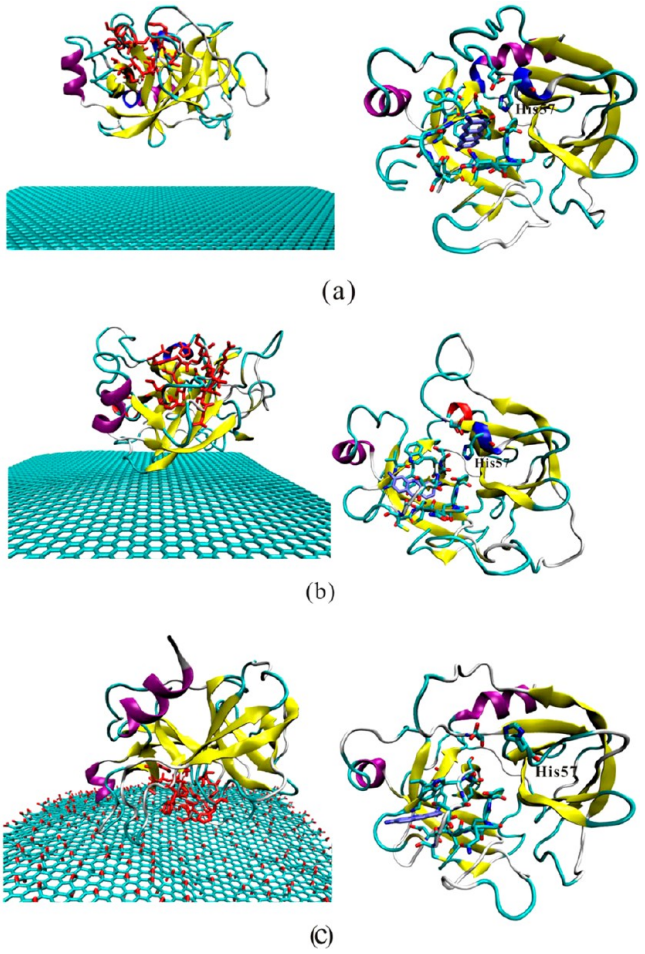

Figure 9. Conformations of the active sites of (a) trypsin in the crystal structure, (b) trypsin absorbed onto the graphene surface, and (c) trypsin absorbed onto the GO surface.

with the structure absorbed onto GO cannot interact with the catalytic triad any more, and the whole ligand can only be found in the right region of the active site.

By comparing the active sites of ChT and trypsin, we find the reason: four residues at positions 189, 192, 217, and 219 are not conserved in trypsin and ChT. Furthermore, Ser190 adopts a different orientation in each of these enzymes as well, pointing into the S1 site of trypsin but away from this site in ChT where it forms a hydrogen bond with Thr138. The bottom of the S1 site in trypsin contains Asp189 which is anionic at neutral pH and can stabilize the positive charge of lysine/arginine residues for which trypsin has displayed a preference. The S1 pocket of ChT on the other hand does not contain this aspartate anion but is uniquely fitted for accepting hydrophobic residues as it is formed from Ser189, Ser190, Ser195, Met192, Trp215, Gly216, Ser217, and Gly226.

Our results indicate the importance of cationic residues of ChT/trypsin to interact with GO and ChT, and show that trypsin share similar interaction modes with GO.

CONCLUSION

In this study, we explore the interactions between enzymes and graphene and GO by the MD simulations. Our results show that ChT can be adsorbed onto the surfaces of both graphene and GO with different surface curvature and area. Moreover, the S1 specificity pocket in ChT is far away from the graphene surface, while it is adsorbed onto the GO surface by its cationic residues and hydrophilic residues, which strongly inhibits enzymatic activity. By careful examination, we observe that the position and conformation of the S1 specificity pocket are the reason that GO exhibited the good capability to inhibitor ChT: the S1 specificity pocket of ChT is not available for ligands due to large conformational changes upon absorption onto GO, while it is available for ligand because it only undergoes small conformational change when adsorbed onto graphene. Importantly, we obtain similar results for trypsin. Our study shows the position and conformation of the S1 specificity pocket is important for enzymatic activity. Our results indicate useful guides for designing nanoparticles to interact with enzymes.

ASSOCIATED CONTENT

Supporting Information

Figure S1 shows typical structure of α-chymotrypsin adsorbed on the graphene surface and the GO surface in other two simulations; Figure S2 shows the active pocket of α-chymotrypsin; Figure S3 shows the active site of α-chymotrypsin during our simulations with graphene sheet or with GO sheet. This material is available free of charge via the Internet at http://pubs.acs.org.

AUTHOR INFORMATION

Corresponding Author

*E-mail: yyli@suda.edu.cn. Phone: +86-512-65882037.

Author Contributions

†X.S. and Z.F. contributed equally to this report.

Notes

The authors declare no competing financial interest.

ACKNOWLEDGMENTS

This work was supported by the National Basic Research Program of China (973 Program, Grant 2012CB932400), the National Natural Science Foundation of China (Grants 91233115, 21273158, and 91227201), and a Project Funded by the Priority Academic Program Development of Jiangsu Higher Education Institutions (PAPD). This is also a project supported by the Fund for Innovative Research Teams of Jiangsu Higher Education Institutions.

REFERENCES

(1) Jin, L.; Yang, K.; Yao, K.; Zhang, S.; Tao, H.; Lee, S. T.; Liu, Z.; Peng, R. Functionalized Graphene Oxide in Enzyme Engineering: A Selective Modulator for Enzyme Activity and Thermostability. *ACS Nano* **2012**, *6*, 4864−4875.

(2) Kirk, O.; Borchert, T. V.; Fuglsang, C. C. Industrial Enzyme Applications. *Curr. Opin. Biotechnol.* **2002**, *13*, 345−351.

(3) Sahoo, D.; Bhattacharya, P.; Patra, H. K.; Mandal, P.; Chakravorti, S. Gold Nanoparticle Induced Conformational Changes in Heme Protein. *J. Nanopart. Res.* **2011**, *13*, 6755−6760.

(4) Thompson, A. B.; Calhoun, A. K.; Smagghe, B. J.; Stevens, M. D.; Wotkowicz, M. T.; Hatziioannou, V. M.; Bamdad, C. A Gold Nanoparticle Platform for Protein−Protein Interactions and Drug Discovery. *ACS Appl. Mater. Interfaces* **2011**, *3*, 2979−2987.

(5) Walkey, C. D.; Olsen, J. B.; Guo, H.; Emili, A.; Chan, W. C. W. Nanoparticle Size and Surface Chemistry Determine Serum Protein Adsorption and Macrophage Uptake. *J. Am. Chem. Soc.* **2012**, *134*, 2139−2147.

(6) Yang, W.; Sun, L.; Weng, J.; Chen, L.; Zhang, Q. Probing the Interaction of Bovine Haemoglobin with Gold Nanoparticles. *IET Nanobiotechnol.* **2012**, *6*, 26−32.

(7) Aubin-Tam, M. E.; Hamad-Schifferli, K. Structure and Function of Nanoparticle−Protein Sonjugates. *Biomed. Mater.* **2008**, *3*, 034001.
(8) Vangala, K.; Ameer, F.; Salomon, G.; Le, V.; Lewis, E.; Yu, L.; Liu, D.; Zhang, D. Studying Protein and Gold Nanoparticle Interaction Using Organothiols as Molecular Probes. *J. Phys. Chem. C* **2012**, *116*, 3645−3652.
(9) Konwarh, R.; Karak, N.; Rai, S. K.; Mukherjee, A. K. Polymer-Assisted Iron Oxide Magnetic Nanoparticle Immobilized Keratinase. *Nanotechnology* **2009**, *20*, 225107.
(10) Li, J.; Wang, J.; Gavalas, V. G.; Atwood, D. A.; Bachas, L. G. Alumina-Pepsin Hybrid Nanoparticles with Orientation-Specific Enzyme Coupling. *Nano Lett.* **2003**, *3*, 55−58.
(11) Yang, Z.; Si, S.; Zhang, C. Study on the Activity and Stability of Urease Immobilized onto Nanoporous Alumina Membranes. *Micropor. Mesopor. Mater.* **2008**, *111*, 359−366.
(12) Lei, C.; Shin, Y.; Liu, J.; Ackerman, E. J. Entrapping Enzyme in a Functionalized Vanoporous Support. *J. Am. Chem. Soc.* **2002**, *124*, 11242−11243.
(13) Luckarift, H. R.; Spain, J. C.; Naik, R. R.; Stone, M. O. Enzyme Immobilization in a Biomimetic Silica Support. *Nat. Biotechnol.* **2004**, *22*, 211−213.
(14) Lee, C. H.; Lin, T. S.; Mou, C. Y. Mesoporous Materials for Encapsulating Enzymes. *Nano Today* **2009**, *4*, 165−179.
(15) Kim, J.; Grate, J. W.; Wang, P. Nanostructures for Enzyme Stabilization. *Chem. Eng. Sci.* **2006**, *61*, 1017−1026.
(16) Takahashi, H.; Li, B.; Sasaki, T.; Miyazaki, C.; Kajino, T.; Inagaki, S. Catalytic Activity in Organic Solvents and Stability of Immobilized Enzymes Depend on the Pore Size and Surface Characteristics of Mesoporous Silica. *Chem. Mater.* **2000**, *12*, 3301−3305.
(17) Bornscheuer, U. T. Immobilizing Enzymes: How to Create More Suitable Biocatalysts. *Angew. Chem., Int. Ed.* **2003**, *42*, 3336−3337.
(18) Lin, Y.; Lu, F.; Tu, Y.; Ren, Z. Glucose Biosensors Based on Carbon Nanotube Nanoelectrode Ensembles. *Nano Lett.* **2004**, *4*, 191−195.
(19) Lee, Y. M.; Kwon, O. Y.; Yoon, Y. J.; Ryu, K. Immobilization of Horseradish Peroxidase on Multi-Wall Carbon Nanotubes and its Electrochemical Properties. *Biotechnol. Lett.* **2006**, *28*, 39−43.
(20) Whitby, R. L. D.; Gun'ko, V. M.; Korobeinyk, A.; Busquets, R.; Cundy, A. B.; László, K.; Skubiszewska-Zięba, J.; Leboda, R.; Tombácz, E.; Toth, I. Y. Driving Forces of Conformational Changes in Single-Layer Graphene Oxide. *ACS Nano* **2012**, *6*, 3967.
(21) Zhang, J.; Zhang, F.; Yang, H.; Huang, X.; Liu, H.; Guo, S. Graphene Oxide as a Matrix for Enzyme Immobilization. *Langmuir* **2010**, *26*, 6083−6085.
(22) Lu, N.; Yin, D.; Li, Z.; Yang, J. Structure of Graphene Oxide: Thermodynamics versus Kinetics. *J. Phys. Chem. C* **2011**, *115*, 11991−11995.
(23) Shih, C. J.; Lin, S.; Sharma, R.; Strano, M. S.; Blankschtein, D. Understanding the pH-Dependent Behavior of Graphene Oxide Aqueous Solutions: A Comparative Experimental and Molecular Dynamics Simulation Study. *Langmuir* **2011**, *28*, 235−241.
(24) Bianco, A.; Kostarelos, K.; Prato, M. Applications of Carbon Nanotubes in Drug Delivery. *Curr. Opin. Chem. Biol.* **2005**, *9*, 674−679.
(25) Sun, X.; Liu, Z.; Welsher, K.; Robinson, J. T.; Goodwin, A.; Zaric, S.; Dai, H. Nano-Graphene Oxide for Cellular Imaging and Drug Delivery. *Nano Res.* **2008**, *1*, 203−212.
(26) Stiriba, S. E.; Frey, H.; Haag, R. Dendritic Polymers in Biomedical Applications: from Potential to Clinical Use in Diagnostics and Therapy. *Angew. Chem., Int. Ed.* **2002**, *41*, 1329−1334.
(27) Wang, J.; Lin, Y. Functionalized Carbon Nanotubes and Nanofibers for Biosensing Applications. *TrAC, Trend. Anal. Chem.* **2008**, *27*, 619−626.
(28) Li, Q.; Mahendra, S.; Lyon, D. Y.; Brunet, L.; Liga, M. V.; Li, D.; Alvarez, P. J. Antimicrobial Nanomaterials for Water Disinfection and Microbial Control: Potential Applications and Implications. *Water Res.* **2008**, *42*, 4591−4602.
(29) Wang, W.; Donini, O.; Reyes, C. M.; Kollman, P. A. Biomolecular Simulations: Recent Developments in Force Fields, Simulations of Enzyme Catalysis, Protein-Ligand, Protein-Protein, and Protein-Nucleic Acid Noncovalent Interactions. *Annu. Rev. Bioph. Biom.* **2001**, *30*, 211−243.
(30) Wen, Y.; Peng, C.; Li, D.; Zhuo, L.; He, S.; Wang, L.; Huang, Q.; Xu, Q.-H.; Fan, C. Metal Ion-Modulated Graphene-DNAzyme Interactions: Design of a Nanoprobe for Fluorescent Detection of Lead (II) Ions with High Sensitivity, Selectivity and Tunable Dynamic Range. *Chem. Commun.* **2011**, *47*, 6278−6280.
(31) De, M.; Chou, S. S.; Dravid, V. P. Graphene Oxide as an Enzyme Inhibitor: Modulation of Activity of α-Chymotrypsin. *J. Am. Chem. Soc.* **2011**, *133*, 17524−17527.
(32) Tsukada, H.; Blow, D. Structure of α-Chymotrypsin Refined at 1.68 Å Resolution. *J. Mol. Biol.* **1985**, *184*, 703−711.
(33) Gaboriaud, C.; Serre, L.; Guy-Crotte, O.; Forest, E.; Fontecilla-Camps, J. C. Crystal Structure of HumanTrypsin 1: Unexpected Phosphorylation of Tyr151. *J. Mol. Biol.* **1996**, *259*, 995−1010.
(34) Collaboration, D.; Abreu, P. Performance of the DELPHI Detector. *Nucl. Instrum. Meth. Phys. Res., Sect. A* **1996**, *378*, 57−100.
(35) Søndergaard, C. R.; Olsson, M. H.; Rostkowski, M.; Jensen, J. H. Improved treatment of ligands and coupling effects in empirical calculation and rationalization of p K a values. *J. Chem. Theory Comput.* **2011**, *7*, 2284−2295.
(36) Anandakrishnan, R.; Aguilar, B.; Onufriev, A. V. H++ 3.0: automating pK prediction and the preparation of biomolecular structures for atomistic molecular modeling and simulations. *Nucleic Acids Res.* **2012**, *40*, W537−W541.
(37) Cruickshank, W. H.; Kaplan, H. A competitive labelling method for determining the ionization constants and reactivity of individual histidine residues in proteins. The histidines of alpha-chymotrypsin. *Biochem. J.* **1972**, *130*, 1125−1131.
(38) Neidhart, D.; Wei, Y.; Cassidy, C.; Lin, J.; Cleland, W. W.; Frey, P. A. Correlation of Low-Barrier Hydrogen Bonding and Oxyanion Binding in Transition State Analogue Complexes of Chymotrypsin. *Biochemistry* **2001**, *40*, 2439−2447.
(39) Kossiakoff, A. A.; Spencer, S. A. Direct determination of the protonation states of aspartic acid-102 and histidine-57 in the tetrahedral intermediate of the serine proteases: neutron structure of trypsin. *Biochemistry* **1981**, *20*, 6462−6474.
(40) Lin, J.; Cassidy, C. S.; Frey, P. A. Correlations of the basicity of His 57 with transition state analogue binding, substrate reactivity, and the strength of the low-barrier hydrogen bond in chymotrypsin. *Biochemistry* **1998**, *37*, 11940−11948.
(41) Medhekar, N. V.; Ramasubramaniam, A.; Ruoff, R. S.; Shenoy, V. B. Hydrogen Bond Networks in Graphene Oxide Composite Paper: Structure and Mechanical Properties. *ACS Nano* **2010**, *4*, 2300−2306.
(42) Argyris, D.; Tummala, N. R.; Striolo, A.; Cole, D. R. Molecular Structure and Dynamics in Thin Water Films at the Silica and Graphite Surfaces. *J. Phys. Chem. C* **2008**, *112*, 13587−13599.
(43) Patra, N.; Wang, B.; Král, P. Nanodroplet Activated and Guided Folding of Graphene Nanostructures. *Nano Lett.* **2009**, *9*, 3766−3771.
(44) Gourlay, M. D.; Kendrick, J.; Leusen, F. J. Rationalization of Racemate Resolution: Predicting Spontaneous Resolution through Crystal Structure Prediction. *Cryst. Growth Des.* **2007**, *7*, 56−63.
(45) Künzel, D.; Markert, T.; Groß, A.; Benoit, D. M. Bis (Terpyridine)-Based Surface Template Structures on Graphite: a Force Field and DFT Study. *Phys. Chem. Chem. Phys.* **2009**, *11*, 8867−8878.
(46) Bikadi, Z.; Hazai, E. Application of the PM6 Semi-Empirical Method to Modeling Proteins Enhances Docking Accuracy of AutoDock. *J. Cheminformatics* **2009**, *1*, 1−15.
(47) Hummer, G.; Rasaiah, J. C.; Noworyta, J. P. Water Conduction through the Hydrophobic Channel of a Carbon Nanotube. *Nature* **2001**, *414*, 188−190.
(48) Jorgensen, W. L.; Chandrasekhar, J.; Madura, J. D.; Impey, R. W.; Klein, M. L. Comparison of Simple Potential Functions for Simulating Liquid Water. *J. Chem. Phys.* **1983**, *79*, 926.

(49) Hsin, J.; Arkhipov, A.; Yin, Y.; Stone, J. E.; Schulten, K. Using VMD: an Introductory Tutorial. *Curr. Protoc. Bioinform.* **2008**, *7*, 1−5.
(50) Kalé, L.; Skeel, R.; Bhandarkar, M.; Brunner, R.; Gursoy, A.; Krawetz, N.; Phillips, J.; Shinozaki, A.; Varadarajan, K.; Schulten, K. NAMD2: Greater Scalability for Parallel Molecular Dynamics* 1. *J. Comput. Phys.* **1999**, *151*, 283−312.
(51) Brooks, B. R.; Bruccoleri, R. E.; Olafson, B. D. CHARMM: A Program for Macromolecular Energy, Minimization, and Dynamics Calculations. *J. Comput. Chem.* **1983**, *4*, 187−217.
(52) MacKerell, A. D.; Bashford, D.; Bellott, M.; Dunbrack, R. L.; Evanseck, J. D.; Field, M. J.; Fischer, S.; Gao, J.; Guo, H.; Ha, S.; Joseph-McCarthy, D.; Kuchnir, L.; Kuczera, K.; Lau, F. T. K.; Mattos, C.; Michnick, S.; Ngo, T.; Nguyen, D. T.; Prodhom, B.; Reiher, W. E.; Roux, B.; Schlenkrich, M.; Smith, J. C.; Stote, R.; Straub, J.; Watanabe, M.; Wiorkiewicz-Kuczera, J.; Yin, D.; Karplus, M. All-atom empirical potential for molecular modeling and dynamics studies of proteins. *J. Phys. Chem. B* **1998**, *102*, 3586−3616.
(53) Feller, S. E.; MacKerell, A. D. An Improved Empirical Potential Energy Function for Molecular Simulations of Phospholipids. *J. Phys. Chem. B* **2000**, *104*, 7510−7515.
(54) Essmann, U.; Perera, L.; Berkowitz, M. L.; Darden, T.; Lee, H.; Pedersen, L. G. A Smooth Particle Mesh Ewald Method. *J. Chem. Phys.* **1995**, *103*, 8577−8593.
(55) Zuo, G.; Zhou, X.; Huang, Q.; Fang, H.; Zhou, R. Adsorption of Villin Headpiece onto Graphene, Carbon Nanotube, and C60: Effect of Contacting Surface Curvatures on Binding Affinity. *J. Phys. Chem. C* **2011**, *115*, 23323−23328.
(56) Katoch, J.; Kim, S. N.; Kuang, Z.; Farmer, B. L.; Naik, R. R.; Tatulian, S. A.; Ishigami, M. Structure of a Peptide Adsorbed on Graphene and Graphite. *Nano Lett.* **2012**, *12*, 2342−2346.
(57) Zuo, G.; Huang, Q.; Wei, G.; Zhou, R.; Fang, H. Plugging into Proteins: Poisoning Protein Function by a Hydrophobic Nanoparticle. *ACS Nano* **2010**, *4*, 7508−7514.
(58) Shen, J. W.; Wu, T.; Wang, Q.; Kang, Y. Induced Stepwise Conformational Change of Human Serum Albumin on Carbon Nanotube Surfaces. *Biomaterials* **2008**, *29*, 3847−3855.
(59) Friling, S.; Notman, R.; Walsh, T. R. Probing Diameter-Selective Solubilisation of Carbon Nanotubes by Reversible Cyclic Peptides using Molecular Dynamics Simulations. *Nanoscale* **2009**, *2*, 98−106.
(60) Calvaresi, M.; Zerbetto, F. Baiting Proteins with C60. *ACS Nano* **2010**, *4*, 2283−2299.
(61) Frampton, M. B.; Zelisko, P. M. A Comparison of Protease Active Sites and their Ability to Process Silicon-Based Substrates. *Silicon* **2012**, *4*, 51−56.
(62) Zsila, F.; Iwao, Y. The Drug Dinding Site of Human α_1-Acid Glycoprotein: Insight from Induced Circular Dichroism and Electronic Absorption Spectra. *Biochem. Biophys. Acta* **2007**, *1770*, 797−809.
(63) Zsila, F.; Kámán, J.; Bogányi, B.; Józsvai, D. Binding of Alkaloids into the S1 Specificity Pocket of α-Chymotrypsin: Evidence from Induced Circular Dichroism Spectra. *Org. Biomol. Chem.* **2011**, *9*, 4127−4137.